American Mineralogist, Volume 87, pages 1261–1265, 2002

Structural refinements of magnesite at very high pressure

GUILLAUME FIQUET,[1,*] FRANÇOIS GUYOT,[1] MARTIN KUNZ,[2] JAN MATAS,[3] DENIS ANDRAULT,[4] AND MICHAEL HANFLAND[5]

[1]Laboratoire de Minéralogie Cristallographie,UMR CNRS 7590, Institut de Physique du Globe de Paris, Universités Paris VI et VII, 4 Place Jussieu, 75252 Paris cedex 05 France
[2]Naturhistorisches Museum, Augustinergasse 2, CH-4001 Basel
[3]Laboratoire de Sciences de la Terre, Ecole Normale Supérieure de Lyon, 46, Allée d'Italie 69364 LYON Cedex 07 France
[4]Département des Géomatériaux, Institut de Physique du Globe de Paris, 4 Place Jussieu, 75252 Paris Cedex 05 France
[5]ESRF - High-pressure group, 6 rue Jules Horowitz BP220, 38043 Grenoble Cedex France

ABSTRACT

Unit-cell parameters of magnesite were measured between ambient pressure and 80 GPa using angle dispersive powder X-ray diffraction. The isothermal bulk modulus determined from a third order Birch Murnaghan equation of state is K_T = 108(3) GPa with K_T' = 5.0(2), and V_0 = 279.2(2) Å^3, in agreement with previously reported values. Combining this result with previous measurements, we show that magnesite with $R\bar{3}c$ structure is stable compared to the assemblage periclase + carbon dioxide at pressures and temperatures corresponding to the core-mantle boundary. Crystal structure refinements have also been carried out up to 80 GPa. The main structural change is a strong compression of the MgO_6 octahedra with increasing pressure, largely reflected in the anisotropic compression of the **c** axis. This compression, however, tends to level off at around 50–60 GPa. On the other hand, the CO_3 groups do not remain invariant since they undergo first a slight expansion and then a compression above the same threshold pressure of 60 GPa above which Mg-O bonds cannot compress further. Thus, in this structure-type, the energy gain due to a drastic volume reduction of the MgO_6 octahedron compensates in a given pressure range for the energy cost of the small expansion of the CO_3 carbonate unit.

INTRODUCTION

There have been a considerable number of studies suggesting that magnesite should be considered when evaluating the role of carbon in the Earth's mantle. Magnesite ($MgCO_3$) is indeed a very good candidate for hosting oxidized carbon in the mantle, since experiments or calculations indicate that magnesite is, among all carbonates, the most stable at high-pressure and high-temperature (e.g., Katsura et al. 1991; Katsura and Ito 1990; Biellmann et al. 1993; Gillet 1993; Martinez et al. 1998). Numerous experiments have been dedicated to determining the compression properties (i.e., bulk modulus and its pressure derivative) of magnesite, as these govern to some extent its stability versus decomposition into a mixture of the oxides MgO and CO_2 (Redfern et al. 1993; Fiquet et al. 1994; Zhang et al. 1997; Ross 1997; Fiquet and Reynard 1999). The structural refinement of Ross (1997), however, was only carried out to 8 GPa. Here, we extend the knowledge of this crystal structure over a larger pressure domain. The high-pressure behavior of magnesite ($MgCO_3$) has been studied by angle dispersive X-ray diffraction up to 81 GPa. The combination of a bright focused monochromatic beam and a two dimensional detection system (imaging plates) allowed us to carry out a structural study of magnesite above 80 GPa.

EXPERIMENTAL DETAILS

Clear inclusion-free crystals from Bahia magnesite, similar to those used in Humbert and Plicque's (1972) ultrasonic study as well as Fiquet and Reynard's (1999) X-ray diffraction study, were chosen for this work. Samples were powdered in an agate mortar and placed in a diamond-anvil cell (Chervin et al. 1994) equipped with type Ia beveled diamonds with 100 μm inner diameter culets. No pressure transmitting medium was used to avoid any chemical reaction. Magnesite crystals were intimately mixed with powdered platinum (platinum black) used as internal pressure calibrant as well as infrared absorber (Jamieson et al. 1982; Holmes et al. 1989). At each pressure increase, the sample was thoroughly annealed with a multi-mode infrared YAG (cw 280 W from Lee lasers) by focusing the laser beam into a 50 μm hot spot and scanning it across the sample for several minutes. The resulting local heating in the temperature range 2000–2500 K is enough to (1) release deviatoric stresses accumulated during the compression at ambient temperature and (2) promote any possible phase transition or decomposition. This annealing is very important since it results in a dramatic release of deviatoric stress, from a value of more than 2 GPa after cold compression to about 0.5 GPa after heating at 80 GPa. This is also evidenced by a factor of two reduction of the line widths during laser heating. The diamond-anvil cell was then mounted on the diffractometer at the ESRF high-pressure beamline ID09. A focused monochromatic beam (wavelength λ = 0.4561 Å) was used in combination with imaging

* E-mail: fiquet@lmcp.jussieu.fr

plates located 450 mm from the sample. Typical exposure times were on the order of 5–10 min with the machine operating at 190 mA in 2/3 filling mode. The imaging plates were scanned with an off-line Molecular Dynamic STORM scanner. Some patterns were also recorded at the ESRF high-pressure beamline ID30, with a focused monochromatic beam (wavelength λ = 0.3738 Å) combined with a "FastScan" on-line imaging plate reader (Thoms et al. 1998) located 350 mm from the sample. The images were corrected for spatial distortion and flat field effects, and subsequently integrated with the Fit2d software (Hammersley 1996), taking into account polarization of the beam. The one dimensional integrated patterns were then treated with the GSAS package, first using the LeBail approach to fix instrumental parameters, peak profile function, and unit-cell dimensions before applying a full scale Rietveld refinement up to 80 GPa (see Fig. 1).

RESULTS

Lattice parameters are reported as a function of pressure in Table 1. A third-order Eulerian equation of states fitted to this compression data set combined with a subset from Fiquet and Reynard (1999) of data recorded in a quasi-hydrostatic environment (using argon and the methanol:ethanol:water mixture as pressure transmitting medium) yields a bulk modulus of 108 (3) GPa and a first pressure derivative K_0' of 5.0 ± 0.2 with a room-pressure molar volume of 279.2 (2) Å. These results are in good agreement with the data of Ross (1997) for the bulk modulus, but the extended pressure range definitely gives a better constraint on the first pressure derivative K_0'. The pressure derivative K_0' is 4.7 ± 0.1 when the bulk modulus is fixed to the value of 112 GPa derived from the ultrasonic measurements of Humbert and Plicque (1972). These equations of state are plotted against experimental data in Figure 2.

As shown in Figure 2, we also observe a large anisotropy in axial compressibility, the *c* axis being three times more compressible than the *a* axis. This feature has already been observed for magnesite (Ross 1997; Zhang et al. 1997; Fiquet and Reynard 1999) and other carbonate compounds (e.g., Ross and Reeder 1992; Martinez et al. 1996), although the ratio of compression differs slightly from that reported by Ross (1997). Note however that the pressure range explored here justifies a second order term.

In addition, the quality of the diffraction pattern was high enough to permit Rietveld analyses, which were carried out up to 80 GPa with the GSAS package (Larson and Von Dreele 1994). In these refinements, the thermal parameters U_{iso} were fixed to values from the single crystal study of Ross (1997). No absorption correction was applied. The $R\bar{3}c$ structure of magnesite has three geometrical degrees of freedom, the cell edges *a* and *c* as well as the fractional coordinate *x* of the O atom O. In addition to these parameters, we also refined two profile parameters for the diffraction peaks as well as twelve background coefficients, and one preferred orientation coefficient for magnesite. As explained above, maximum care was taken to eliminate deviatoric stresses as efficiently as possible with the use of the laser annealing. Nevertheless, preferred orientations are unavoidable at very high pressures, but there can be accommodated with a preferred orientation parameter. The results are reported in Table 2 and plotted in Figure 3.

DISCUSSION

Equation of state and high-pressure stability

These measurements shed new light on the stability of magnesite at extreme pressure and temperature conditions. Experi-

TABLE 1. Unit-cell of magnesite to 82.6 GPa

P (GPa)	*a* (Å)	*c* (Å)	*V* (Å³)
23.1(4)	4.4818(3)	13.9150(28)	242.06(4)
29.9(6)	4.4560(5)	13.7092(35)	235.74(5)
41.3(8)	4.4044(3)	13.3797(30)	224.78(4)
45.6(9)	4.3895(4)	13.2938(31)	221.83(4)
51.8(11)	4.3675(3)	13.1387(27)	217.05(4)
56.6(11)	4.3530(4)	13.0325(29)	213.86(4)
60.2(12)	4.3401(3)	12.9538(22)	211.31(3)
70.7(15)	4.3138(3)	12.7762(17)	205.90(2)
71.2(16)	4.3102(5)	12.7451(30)	205.06(4)
75.7(17)	4.2981(3)	12.6690(25)	202.68(3)
82.6(18)	4.2783(4)	12.5461(29)	198.87(4)

Note: Standard deviations in parentheses. Pressures and related uncertainties calculated after the equations of state of platinum (Jamieson et al. 1982; Holmes et al. 1989).

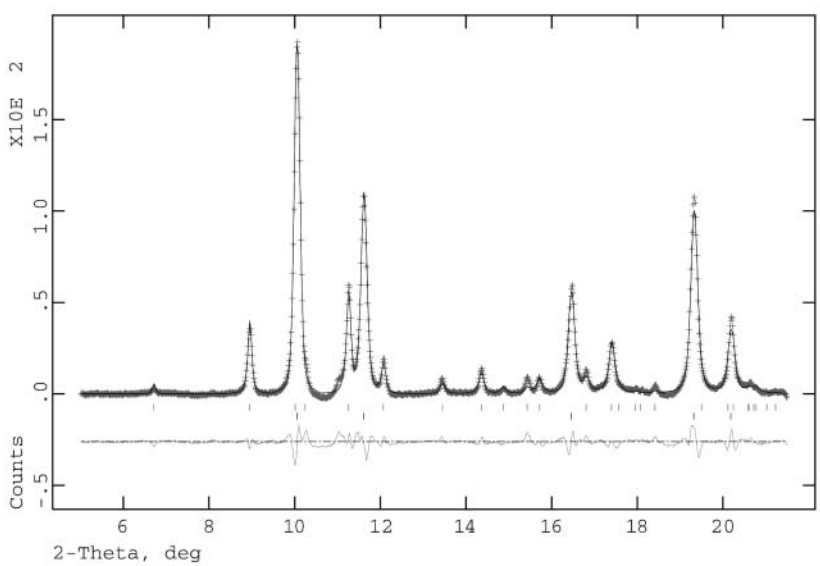

FIGURE 1. A typical example of an X-ray diffraction pattern of a mixture of magnesite and platinum (10% by weight) compressed at 82.6 GPa after laser annealing above 2500 K. Space group $R\bar{3}c$ with a = 4.2783(4) and c = 12.546(3) Å, wR_p = 0.0066, R_p = 0.0042, $R(F^2)$ = 0.0627. The O atom fractional coordinates are [0.2960(11), 0, 1/4]. The background has been subtracted.

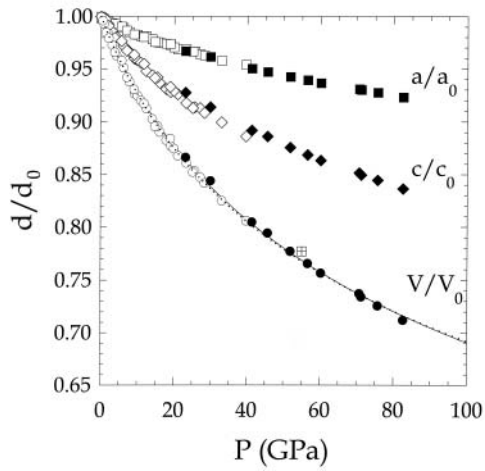

FIGURE 2. The variation of a/a_0, c/c_0, and V/V_0 as a function of pressure plotted along with previous determinations by Katsura et al. (1991) (crossed square) and by Fiquet and Reynard (1999) (open symbols). The best fits to a Birch Murnaghan equation of state are shown as well (K_0 = 112 GPa, K_0' = 4.7, and K_0 = 108 GPa, K_0' = 5 as solid and dotted lines, respectively).

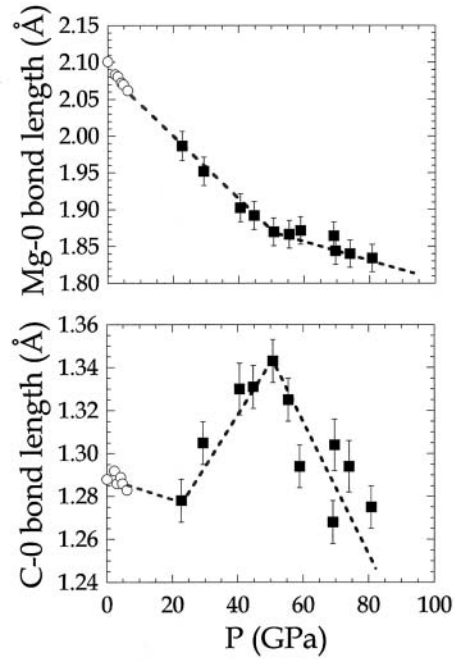

FIGURE 3. Variation of Mg-O and C-O bond lengths as a function of pressure, plotted with data from Ross (1997) to 6 GPa (open circles). Dashed lines are guides for the eye. Note that the error bars have been multiplied by a factor 5 in order to approximate the true uncertainty of Rietveld refinements under these conditions (e.g., Young 1993).

ments show that magnesite with the $R\bar{3}c$ structure is stable at pressures of 80 GPa, in good agreement with previous studies by Katsura et al. (1991) and Gillet (1993). The stability of magnesite in the deep mantle and possible carbon storage at depth can be further evaluated through the chemical reaction:

$$MgCO_3 \rightarrow MgO + CO_2.$$

The equation of state of all three phases must be known as accurately as possible. For CO_2, the high-pressure equation of state of Belonoshko and Saxena (1991) was used along with the enthalpy of formation ΔH_f^0, entropy S_0, and heat capacity C_P given by Robie et al. (1979). For MgO, the entropy and heat capacity calculations reported by Fiquet et al. (1999) and the high-pressure equation of state proposed by Speziale et al. (2001) were used. For magnesite, entropic terms as calculated by Matas et al. (2000) were combined with the equation of state parameters determined in this study. At high pressure, volumetric effects dominate over entropic effects and simple considerations show in the present case that the position of the equilibrium curve is mainly governed by the volume variations of magnesite, i.e., bulk modulus K_0, its pressure derivative K_0', and temperature derivative $(dK/dT)_P$, as shown in Figure 4. Magnesite appears to be stable compared to the assemblage periclase + carbon dioxide over a very large pressure range, i.e., to above 130 GPa. With a K_0 value of 108 GPa, a pressure derivative K_0' of 5, and $(dK/dT)_P$ = –0.017 GPa/K (Zhang et al. 1997), the decarbonation curve does not cross any of the possible lower mantle geotherms (see Fig. 4). On the other hand, such a decarbonation process is highly sensitive to the $(dK/dT)_P$ parameter since a value of $(dK/dT)_P$ = –0.013 GPa/K would be enough to make such decarbonation possible around 120–130 GPa. As already discussed by Martinez et al. (1998), a decarbonation reaction is not the only process affecting the stability of magnesite. Carbonates might indeed undergo melting processes under lower mantle conditions. However, the available experiments (Martinez et al. 1998) have only been performed under the (P,T) conditions of the transition zone.

TABLE 2. Refined positional parameters, interatomic distances (Å) from structure refinements of magnesite at high pressures

P (GPa)	O (x)	Mg-O	C-O	$R(F^2)$
23.1	0.2848(11)	1.9872(22)	1.276(4)	9.40
29.9	0.2926(11)	1.9528(24)	1.304(5)	4.13
41.3	0.3014(13)	1.9040(22)	1.327(5)	6.15
45.6	0.3032(12)	1.8918(24)	1.331(5)	9.53
51.8	0.3073(11)	1.8699(21)	1.342(5)	9.01
56.6	0.3066(12)	1.8620(25)	1.335(5)	8.31
60.2	0.2967(11)	1.8744(23)	1.288(5)	10.49
70.7	0.2919(10)	1.8682(21)	1.259(4)	6.99
71.2	0.3020(15)	1.8452(30)	1.302(6)	9.55
75.7	0.2970(12)	1.8480(25)	1.277(5)	7.33
82.6	0.2960(11)	1.8385(22)	1.266(5)	6.27

Notes: displacement factors B(Å^2) were fixed at 0.38 (Ross 1997). $R(F^2) = \Sigma|F_o^2 - sF_c^2|/\Sigma|F_o^2|$, where s = scale factor, F_o and F_c are the observed and calculated structure factors.

Structural changes with pressure

At ambient conditions, there are two sets of O-O distances, the first corresponding to the O atoms belonging to the carbonate groups (2.23 Å) and the second to a set of O atoms linking different carbonate groups (2.58–2.91 Å), also corresponding to the MgO_6 octahedral edge length. As pressure is increased, the bond lengths display an interesting behavior, with trends well within analytic error bars, as shown in Figure 3. As a first

approximation, the CO_3 groups are rather incompressible rigid units. Unlike the carbonate groups, the MO_6 octahedra undergo a large volume decrease, as evidenced by the large compression along the **c** axis. However, a detailed examination of C-O bond lengths over a wide pressure range indicates that at first they expand before shortening once the Mg-O bonds begin to stiffen at around 60 GPa. To demonstrate this effect more clearly, we use the concept of bond valence (BV), which has found numerous application in solid state chemistry (e.g., Brown and Altermatt 1985; Brese and O'Keeffe 1991). The bond valence S_{ij} of a bond between atoms i and j is calculated by the following empirical expression:

$$S_{ij} = \exp\left(\frac{r_{ij}^0 - d_{ij}}{b}\right) \quad (1)$$

where r_{ij}^0 and b are empirical atom-pair specific parameters determined by the requirement that the sum of all bonds around any given atom must be equal to the atomic valence of the respective atoms. The d_{ij} term represents the distance between the two atoms, i.e., atom i and the neighboring atom j. Bond valence sums as calculated from observed bond distances and Equation 1 are represented at different pressures in Figure 5 for magnesite, with bond valence parameters for Mg^{2+} and O^{2-} (r_0 = 1.693 and b = 0.37) taken from Brown and Altermatt (1985). With compression, the carbonate groups are pushed closer together, and the only force acting against this is the Mg-O bond, which must get shorter. As shown in Figure 5, this leads to a considerable overbonding of the magnesium atoms (BV close to 4 instead of 2) and a overbonding of the O atoms (BV of 3 instead of 2). The lower overbonding of the O atoms is explained by the fact that while the MgO_6 octahedra are compressed, the CO_3 groups are slightly extended. The BV for carbon atoms between 20 and 60 GPa indeed yields sums lower than the ideal value of 4, indicating a "tensional" stress or an underbonding. The overbonding of the O atoms is further alleviated by symmetrizing the O atom surroundings by making the Mg-O and C-O bond lengths more similar. This behavior is in accordance with the distortion theorem based on the exponential relationship between bond valence and bond length

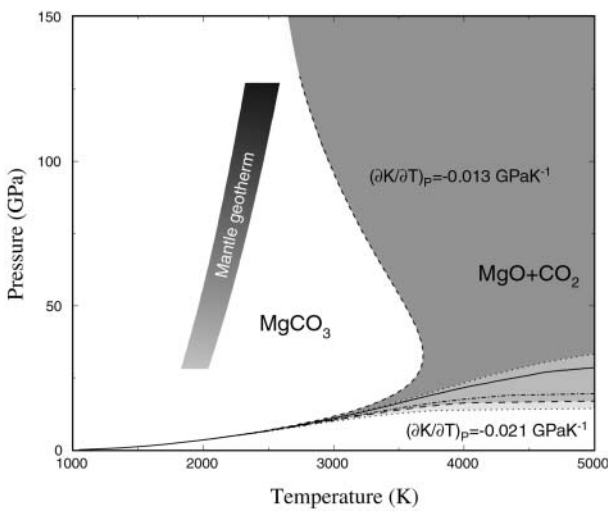

FIGURE 4. The stability curve of magnesite calculated at high pressure and high temperature with different equation of state parameters: a value of $(dK/dT)_P$ = –0.017 GPa/K taken from (Zhang et al. 1997) is combined with K_0 = 108 GPa and K_0' = 5 (solid line), K_0 = 117, and K_0' = 2.3 (dotted dashed line). The effect of uncertainties on the thermal EoS is depicted as shaded areas, i.e., two different values of the parameter $(dK/dT)_P$ are used. These curves are plotted along with different possible temperature profiles in the Earth.

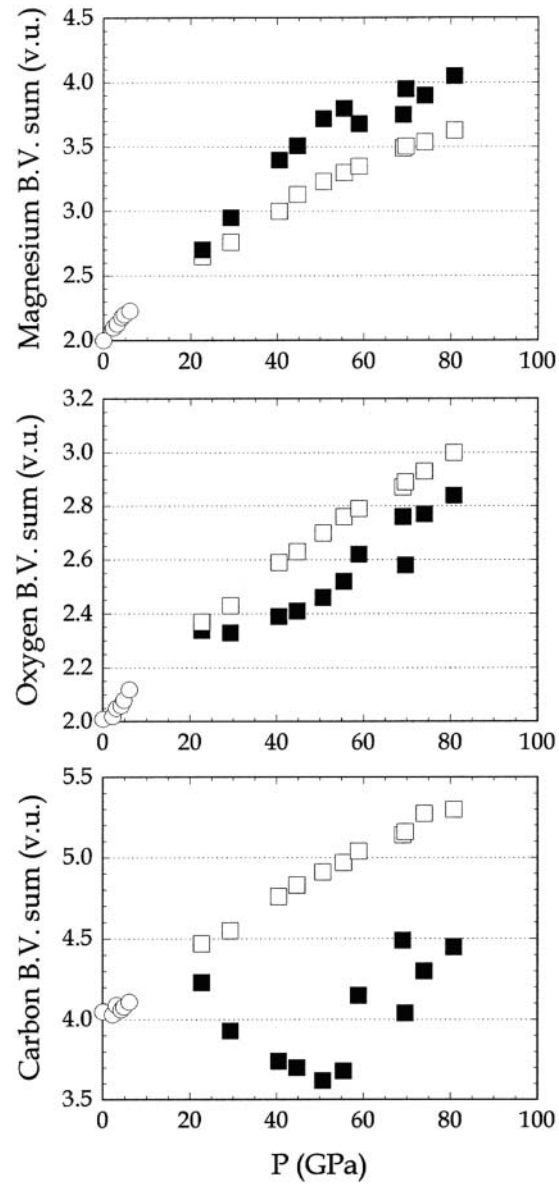

FIGURE 5. BV sums as calculated from observed bond distances using relation (1). Open circles represent values obtained with positional parameters of Ross (1997). Open squares represent values obtained with x(O) = 0.38, solid squares represent values obtained with refined x(O) parameters.

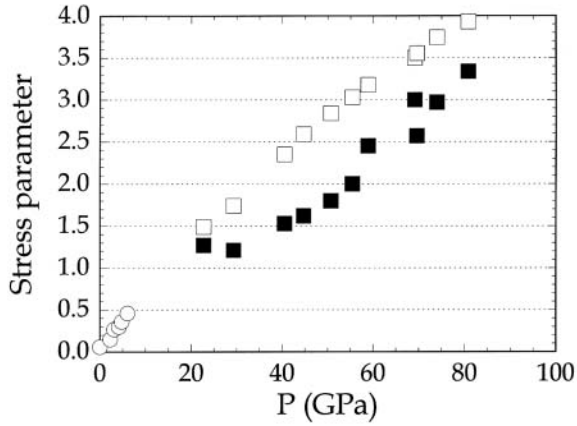

FIGURE 6. This "stress parameter" is calculated as follows: stress parameter = ||BV sum (Mg) – 2|| + ||BV sum (C) – 4|| + ||BV sum (O) – 2||. The open circles represent values obtained using the positional parameters of Ross (1997). The open squares represent values obtained with x(O) = 0.38, and solid squares denote values obtained with refined x(O) parameters.

(Brown 1992). The apparently counter-intuitive expansion of the CO_3 groups with increasing pressure is possible, since the O-O distances between neighboring carbonate groups is large enough, that its effect on the overall volume is over-compensated for by compression of the MgO_6 octahedra. At higher pressures (50–60 GPa), the compression has progressed to an extent that the O-O repulsive forces become more effective and the C-O bond lengths decrease again. That this complicated mechanism is indeed energetically favorable over an isotropic compression of all bond lengths can be demonstrated if one uses the BV sums to define a "stress parameter," as the sum of all differences between observed BV (from measured bond distances) and theoretical atomic valences for Mg, C, and O representing the ideal unstressed state. As can be seen in Figure 6, this parameter is lower if one uses the refined x(O)-coordinates rather than the value of 0.38 as found at low pressure conditions (Ross 1997), which would therefore mimic an isotropic compression. This structure-type thus seems to stabilize its topology at very high pressure by increasing the bond-length of a specific unit (CO_3 groups) at the expense of other more weakly bonded units (MO_6 octahedra). This property might contribute to the remarkable stability of $R\bar{3}c$ magnesite over a very large pressure and temperature range.

ACKNOWLEDGMENTS

T. Le Bihan is warmly acknowledged for his help during experiments carried out at the ESRF ID30 beamline. We thank S. Redfern and one anonymous reviewer for helpful and constructive reviews. This is INSU-CNRS publication number 311.

REFERENCES CITED

Belonoshko, A., and Saxena, S.K. (1991) A molecular dynamics study of the pressure-volume-temperature properties of supercritical fluids: II. CO_2, CH_4, CO, O_2 and H_2. Geochimica Cosmochimica Acta, 55, 3191–3208.

Biellmann, C., Gillet, P., Guyot, F., Peyronneau, J., and Reynard, B. (1993) Experimental evidence for carbonate stability in the Earth's lower mantle. Earth and Planetary Science Letters, 118, 31–41.

Brese, N.E. and O'Keeffe, M. (1991) Bond-valence parameters for solids. Acta Crystallographica, B47, 192–197.

Brown, I.D. (1992) Chemical and steric constraints in inorganic solids. Acta Crystallographica, B48, 553–572.

Brown, I.D. and Altermatt, D. (1985) Bond-valence parameters obtained from a systematic analysis of the inorganic crystal structure database. Acta Crystallographica, B41, 244–247.

Chervin, J.C., Canny, B., Besson, J.M., and Pruzan, Ph. (1994) A diamond-anvil cell for IR microspectroscopy. Reviews of Scientific Instruments, 66, 3, 2595–2598.

Fiquet, G., and Reynard, B. (1999) High-pressure equation of state of magnesite: new data and a reappraisal. American Mineralogist, 84, 856–860.

Fiquet, G., Guyot, F., and Itie, J.P. (1994) High-pressure X-ray diffraction study of carbonates—$MgCO_3$, $CaMg(CO_3)_2$, and $CaCO_3$. American Mineralogist, 79, 15–23.

Fiquet, G., Richet, P., and Montagnac, G. (1999) High-temperature thermal expansion of lime, periclase, corundum and spinel. Physics and Chemistry of Minerals, 27, 103–111.

Gillet, P. (1993) Stability of magnesite ($MgCO_3$) at mantle pressure and temperature conditions. A Raman spectroscopic study. American Mineralogist, 78, 1328–1331.

Hammersley, J. (1996) Fit2d. ESRF publication.

Holmes, N.C., Moriarty, J.A., Gathers, G.R., and Nellis, W.J. (1989) The equation of state of platinum to 660 GPa (6.6 Mbar). Journal of Applied Physics, 66, 2962–2967.

Humbert, P. and Plicque, F. (1972) Propriétés élastiques des carbonates rhombohédriques monocristallins: calcite, magnésite et dolomie. Comptes Rendus de l'Académie des Sciences de Paris, 275, 391–394.

Jamieson, J.C., Fritz, J.N., and Manghnanni, M.H. (1982) Pressure measurement at high temperature in X-ray diffraction study: gold as a primary standard. In S. Akimoto and M.H. Manghnani, Eds., High pressure research in geophysics, Center for academic publications, Tokyo, 27–47.

Katsura, T. and Ito, E. (1990) Melting and subsolidus relations in the $MgSiO_3$-$MgCO_3$ system at high pressures: implications to evolution of the Earth's atmosphere. Earth and Planetary Science Letters, 99, 110–117.

Katsura, T., Tsuchida, Y., Ito, E., Yagi, T., Utsumi, W., and Akimoto, S. (1991) Stability of magnesite under the lower mantle conditions. Proceedings of Japan Academy, 67, B, 4, 57–60.

Larson, A.C. and Von Dreele, R.B. (1994) GSAS manual, report LAUR, Los Alamos National Laboratory, Los Alamos, 86–748.

Martinez, I., Zhang, J., and Reeder, R.J. (1996) In situ x-ray diffraction of aragonite and dolomite at high pressure and high temperature: evidence for dolomite breakdown to aragonite and magnesite, 81, 611–624.

Martinez, I., Chamorro Perez, E.M., Matas, J., Gillet, Ph., and Vidal, G. (1998) Experimental investigation of silicate-carbonate system at high pressure and high temperature. Journal of Geophysical Research, 103, B3, 5143–5163.

Matas, J., Gillet Ph., Ricard, Y., and Martinez, I. (2000) Thermodynamic properties of carbonates at high pressures from vibrational modeling. European Journal of Mineralogy, 12, 4, 703–720.

Redfern, S.A.T., Wood, B.J., and Henderson, C.M.B. (1993) Static compressibility of magnesite to 20 GPa: implications for $MgCO_3$ in the lower mantle. Geophysical Research Letters, 20, 2099–2012.

Robie, R.A., Hemingway, B.S., and Fisher, J.R. (1979) Thermodynamic properties of minerals and related substances at 298.15 K and 1 bar (10^5 pascals) pressure and at higher temperatures. U.S. Geological Survey Bulletin, 1452, 456 p.

Ross, N.L. (1997) The equation of state and high-pressure behavior of magnesite. American Mineralogist, 82, 682–688.

Ross, N.L. and Reeder, R.J. (1992) High-pressure structural study of dolomite and ankerite. American Mineralogist, 77, 412–421.

Speziale, S., Zha, C.S., Duffy, T.S., Hemley, R.J., and Mao, H.K. (2001) Quasi-hydrostatic compression of magnesium oxide to 52 GPa: Implications for the pressure-volume-temperature equation of state. Journal of Geophysical Research, 106, B37, 515–528.

Thoms, M., Häusermann, D., Bauchau, S., Kunz, M., LeBihan, T., Mezouar, M., and Strawbridge, D. (1998) The Fastscan: an on line reader for imaging plates. Nucl. Instrum. Methods, A 143, 175.

Young, R.A. (1993) Introduction to the Rietveld method. In R.A. Young, Ed., The Rietveld Method. IUCr-Oxford Science Publications, Oxford University Press, New York.

Zhang, J., Martinez, I., Guyot, F., Gillet, P., and Saxena, S.K. (1997) X-ray diffraction study of magnesite at high-pressure and high-temperature. Physics and Chemistry of Minerals, 24, 122–130.

MANUSCRIPT RECEIVED DECEMBER 11, 2001
MANUSCRIPT ACCEPTED APRIL 18, 2002
MANUSCRIPT HANDLED BY LEE A. GROAT